J. Fluid Mech. (2003), *vol.* 494, *pp.* 119–140. © 2003 Cambridge University Press
DOI: 10.1017/S0022112003005925 Printed in the United Kingdom

Elliptic jets in cross-flow

By T. H. NEW†, T. T. LIM AND S. C. LUO

Department of Mechanical Engineering, National University of Singapore,
10 Kent Ridge Crescent, Singapore 119260

(Received 3 May 2002 and in revised form 8 May 2003)

Flow structures of an elliptic jet in cross-flow were studied experimentally in a water tunnel using the laser-induced fluorescence technique (LIF), for a range of jet aspect ratio (AR) from 0.3 to 3.0, jet-to-cross-flow velocity ratio (VR) from 1 to 5, and jet Reynolds number from 900 to 5100. The results show that the effects of aspect ratio (or jet exit orientation) are significant only in the near field, and diminish in the far field which depends only on gross jet geometry. For low-aspect-ratio jets, two adjacent counter-rotating vortex pairs (CVP) are initially formed at the sides of the jet column, with the weaker pair subsequently entrained by the stronger pair further downstream. For high-aspect-ratio jets, only one CVP is formed throughout the jet column, but the shear layer develops additional folds along the windward side of the jet. These folds subsequently evolve into smaller scale counter-rotating vortex pairs, which we refer to as windward vortex pairs (WVP). Depending on its sense of rotation, the WVP can evolve into what Haven & Kurosaka (1997) referred to as unsteady kidney vortices or anti-kidney vortices, or, under some circumstances, interconnecting kidney vortices, which have not been reported previously. While Haven & Kurosaka (1997)'s interpretation of the formation of kidney and anti-kidney vortices is topologically feasible, our observation reveals a slightly different formation process. Despite the differences in the near-field flow structures for different jet aspect ratios, the process leading to the formation of the large-scale jet structures (i.e. leading-edge vortices and lee-side vortices) for all cases is similar to that reported by Lim, New & Luo (2001) for a circular jet in cross-flow.

1. Introduction

A jet in cross-flow is a fundamental flow phenomenon that is relevant to many engineering applications, such as film cooling of turbines and combustors, fuel injection of burners, thrust reversers for propulsive systems, V/STOL aircrafts in transition flight, and chimney flow. The flow has attracted the attention of numerous researchers, partly due to its relevance to some fundamental problems in fluid mechanics and partly due to its technological applications.

It is well-established that a circular jet in cross-flow produces a multitude of vortical structures, and the five most significant ones are the leading-edge vortices, lee-side vortices, counter-rotating vortex pairs (CVP), horseshoe vortices and wake vortices (see figure 1). These vortex structures have been studied extensively by many researchers, including Scorer (1958), Kamotani & Greber (1972), Fearn & Weston (1974), Moussa, Trischka & Eskinazi (1977), Coelho & Hunt (1989), Fric & Roshko

† Present address: Temasek Laboratories, National University of Singapore, 10 Kent Ridge Crescent, Singapore 119260.

https://doi.org/10.1017/S0022112003005925 Published online by Cambridge University Press

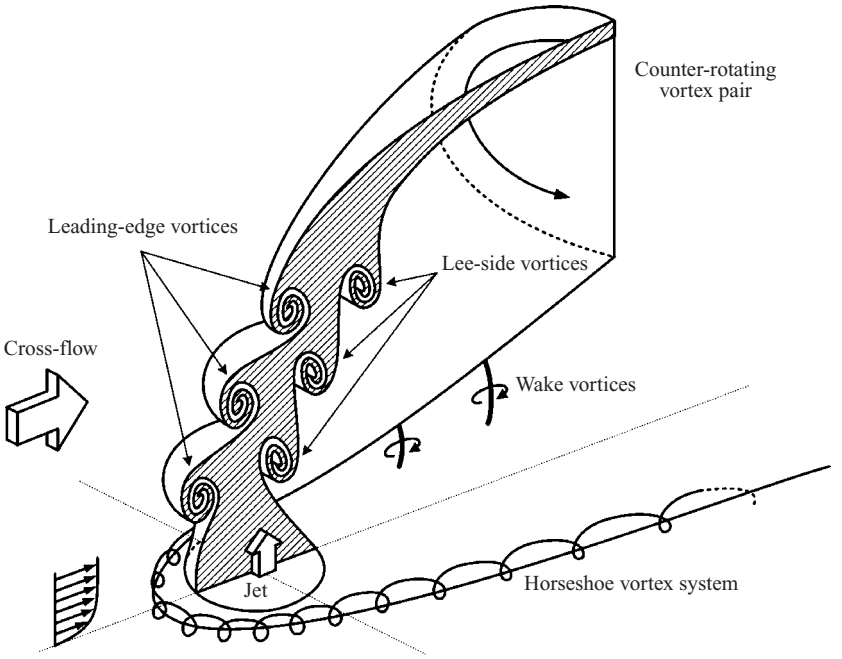


FIGURE 1. Schematic of large-scale vortical structures produced by a circular jet exhausting normally into a cross-flow. Shaded region indicates the cross-section of the deflected jet if a cut is taken along the jet centreline.

(1994), Kelso & Smits (1995), Kelso, Lim & Perry (1996), Haven & Kurosaka (1997), New, Lim & Luo (1999), Yuan, Street & Ferziger (1999) and Lim, New & Luo (2001). The above list is by no means exhaustive and readers should refer to an excellent review article by Margason (1993), which gives a good overview on the whole problem up to 1993.

In recent years, various attempts have been made to improve the mixing efficiency of a jet in cross-flow by using non-circular jet geometry such as an ellipse, square and rectangle (for example, see Haven & Kurosaka 1997; Ajersch *et al.* 1997; Zaman & Foss 1997; Gogineni, Goss & Roquemore 1998; Findlay, Salcudean & Gartshore 1999). Although altering the jet exit geometry has been found to be an effective means of enhancing jet mixing with the surroundings, many fundamental questions about the flow field have not yet been fully answered, particularly those related to the formation of the large-scale jet structures, and their role in the entrainment of the surrounding fluid. These questions are of practical importance in applications such as the design of fuel injectors in burners. In this paper, we focus our investigations on the elliptic jet geometry only. This geometry is chosen for study because it is the simplest of the non-circular jets, and is more stable than square or rectangular jets. Moreover, an elliptic jet has the added advantage of having the smallest possible momentum thickness variation for a symmetrical non-circular jet exit, due to the smooth variation in its perimeter curvature.

An elliptic jet in a cross-flow has been investigated by Haven & Kurosaka (1997), but their study was confined to low velocity ratios (VR) only (i.e. $VR = 0.4$ to 2.0) since they were concerned primarily with the effect of jet geometry on film cooling. The main finding of their investigation is the existence of "double-decked kidney and anti-kidney vortices". They found that the lower-deck structures are kidney-shaped

https://doi.org/10.1017/S0022112003005925 Published online by Cambridge University Press

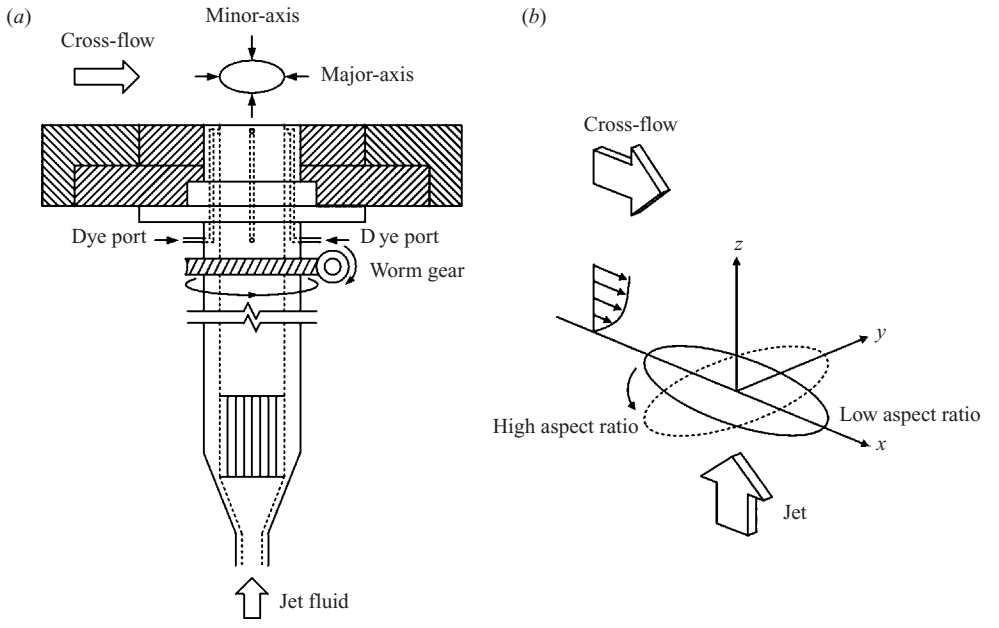


FIGURE 2. (*a*) Jet-supply assembly showing the worm gear fixture. (*b*) Streamwise and cross-stream configuration of the nozzle which correspond to low- and high-AR elliptic jets, respectively.

and established to be the primary CVP inherent in all jet geometries in cross-flow, while the upper-deck structures are dependent on the jet geometry, and could be either unsteady kidney-shaped or unsteady anti-kidney shaped. Accordingly, they classified the flow into two distinct groups: unsteady kidney-shaped for low-aspect-ratio (AR) elliptic jets (i.e. major-axes aligned with the cross-flow), and unsteady anti-kidney shaped for high-AR elliptic jets (i.e. minor-axes aligned with the cross-flow). The fact that their studies were conducted at low VR raises an inevitable question as to whether these unsteady vortices are also prevalent at high VR or are they restricted only to low VR. Addressing this question is one of the motivations of the present investigation. Another motivation is to ascertain whether our vortex skeleton model for a circular jet in cross-flow (see Lim *et al.* 2001) is also applicable to elliptic jets.

2. Experimental apparatus and methods

2.1. *Water tunnel and jet supply setup*

The water tunnel is a re-circulating facility with a Plexiglas test-section measuring 183 cm $(L) \times 40$ cm $(W) \times 45$ cm (H). Before entering the test section, the flow is passed through a honeycomb, three sets of fine screens of decreasing grid size and a 4 : 1 contraction section. This arrangement is to ensure that the turbulence level in the test section is kept to a minimum. The velocity profile taken using a hot-film anemometer at the location of the jet exit (without the jet flow) indicated that the cross-flow boundary layer is laminar.

The jet fluid was supplied from a constant-head tank, which channelled the flow to the jet assembly (see figure 2*a*) through a long rubber hose. The tank was replenished continuously by pumping water from the receiver tank located downstream of the test-section. The jet velocity was controlled by a valve and measured by an electromagnetic

https://doi.org/10.1017/S0022112003005925 Published online by Cambridge University Press

Configuration	Jet exit shape	H (mm)	L (mm)	Aspect ratio (H/L)
1		18.5	55.5	0.3
2		22.5	45	0.5
3		31.6	31.6	1.0
4		45	22.5	2.0
5		55.5	18.5	3.0

TABLE 1. Jet exit geometries used in the present experiment. The arrows denote the cross-flow direction. H is the cross-stream axis and L is the streamwise axis with the aspect ratio defined as H/L.

flow meter. For ease of alignment, the elliptic nozzle is designed to rotate freely about its centreline using a high-gear-ratio worm drive, which enables an accurate alignment of the jet exit relative to the cross-flow. To visualize the flow, food dye was released through selected dye ports located at particular locations around the circumference of the nozzle upstream of the jet exit. On some occasions, dye was also released through a circumferential slit in the jet assembly to allow uniform marking of the entire jet shear layer. To obtain a cross-sectional view of the flow, a thin laser sheet, produced by passing a 5 W Argon-ion laser beam through a cylindrical lens, was used to illuminate the jet fluid that had been premixed with fluorescein disodium dye prior to entering the test section. In all cases, the flow motion was recorded using a SVHS video recorder equipped with a time-code device for subsequent playback and analysis.

2.2. *Key parameters*

A key parameter in this investigation is the aspect ratio (AR) of the jet, which is defined as the ratio of the cross-stream dimension of the nozzle to the streamwise dimension (see table 1). For example, $AR < 1$ implies that the major axis of the ellipse is aligned with the cross-flow, and correspondingly, $AR > 1$ refers to the case where the major axis is normal to the cross-flow. For convenience, jets with $AR < 1$ are labelled as low-AR jets and those with $AR > 1$ are referred to high-AR jets (see also figure 2*b*). The jet exit areas are the same in all cases. Another parameter is the momentum ratio (MR), which can be expressed mathematically as

$$MR = \frac{\int \rho_{jet} V_{jet}^2 \, \mathrm{d}A}{\rho_\infty U_\infty^2 A_{jet}},$$

where ρ_{jet}, V_{jet} and A_{jet} are the density, velocity and cross-sectional area of the jet, respectively, and ρ_∞ and U_∞ are the density and velocity of the cross-flow. However, if the jet and the cross-flow have the same density, and provided that V_{jet} is the mean jet velocity, then the square root of MR reduces to V_{jet}/U_∞, which is commonly referred to as the velocity ratio (VR). In the present study, VR ranges from 1 to 5.

3. Results and discussion

The following discussion concentrates primarily on low- and high-AR elliptic jets; the results for the circular jet will not be presented since they have already been

https://doi.org/10.1017/S0022112003005925 Published online by Cambridge University Press

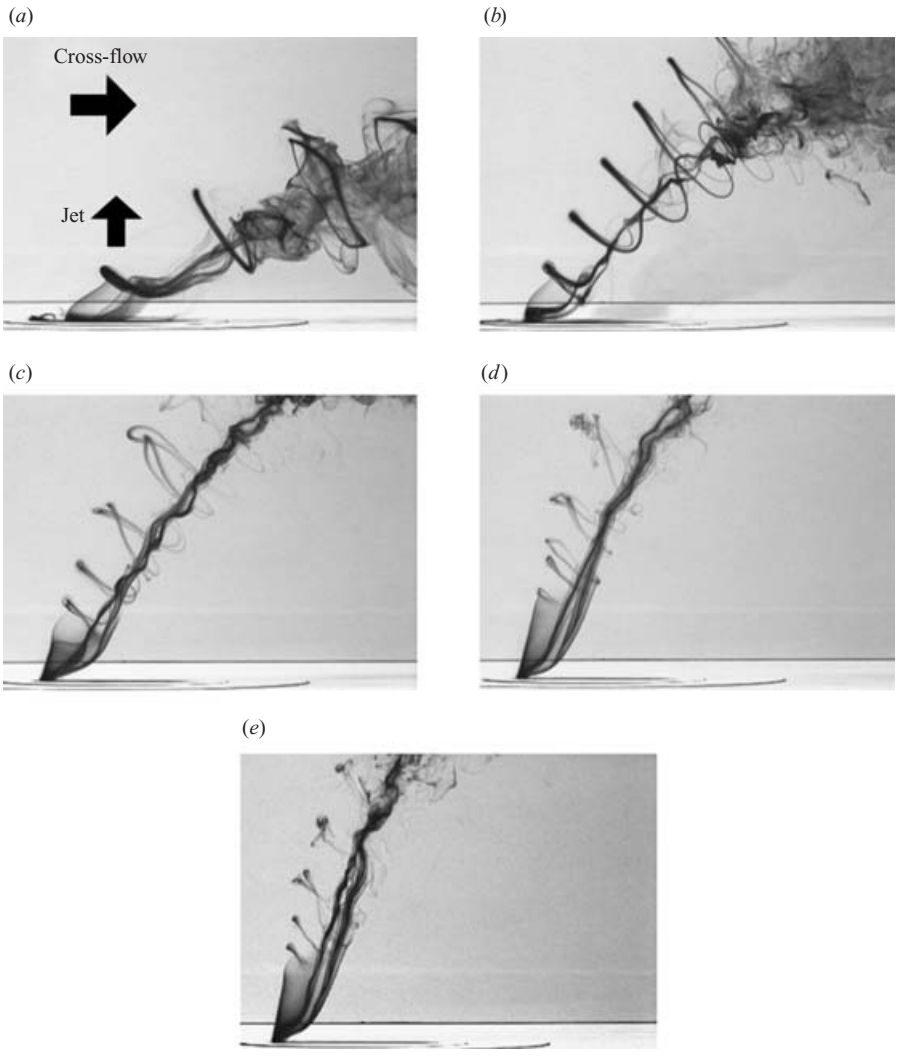


FIGURE 3. Dye pattern of an $AR = 0.3$ jet in cross-flow. The dye was released through a dye port located slightly upstream of the jet exit. (*a*) $VR = 1$, (*b*) $VR = 2$, (*c*) $VR = 3$, (*d*) $VR = 4$, (*e*) $VR = 5$.

reported in Lim *et al.* (2001). However, results for the circular jet will be referred to when necessary to illustrate certain pertinent flow differences between circular and elliptic jets in cross-flow.

3.1. *Low-aspect-ratio elliptic jets in cross-flow*

Figure 3 shows a sequence of flow images for a low-AR jet (i.e. $AR = 0.3$) subjected to a range of velocity ratios. These images were obtained by upstream point injection of coloured dye and clearly show the formation of the CVP and leading-edge vortices, which appear to form periodically, even though no deliberate forcing was applied to the flow. It can also be seen that increasing VR intensified the interaction between neighbouring leading-edge vortices, which subsequently led to their entanglement and pairing further downstream. The process of vortex pairing is more prevalent here than in a circular jet, and can be attributed to the higher curvature of the leading-edge

https://doi.org/10.1017/S0022112003005925 Published online by Cambridge University Press

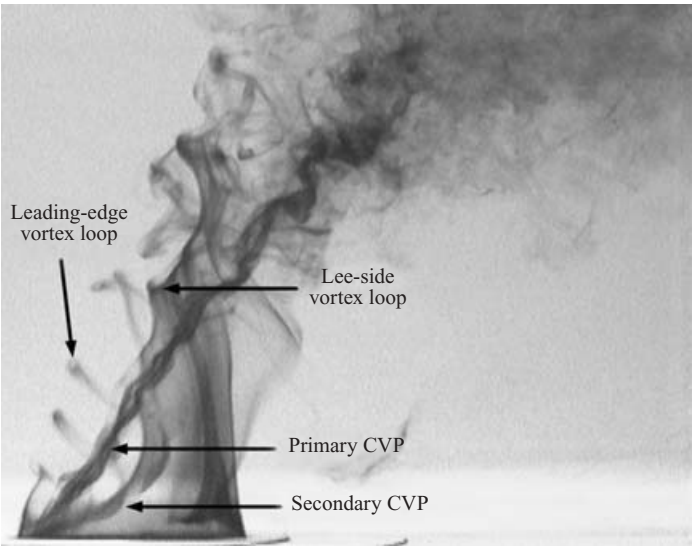


FIGURE 4. Overall view of an $AR = 0.3$ (with $VR = 3$) jet when dye was also released through a circumferential slit upstream of the jet exit. Note that the first lee-side vortex is generated significantly downstream from the first leading-edge vortex.

vortex filaments, and the higher frequency of vortex shedding at higher VR. The phenomenon of axis-switching, which is often observed for an isolated elliptic vortex ring in a quiescent environment, is not observed here. This finding reinforces our earlier observation for a circular jet in cross-flow (see Lim *et al.* 2001) that vortex rings are not the building block of the large-scale structures in jets in cross-flow (i.e. leading-edge and lee-side vortices), even though they are the dominant structures in a free jet. The absence of the vortex rings in a jet in cross-flow can be attributed to the presence of the CVP at the side of the jet column, which prevented the rings from forming. Instead, a jet in cross-flow is dominated by a daisy chain of interconnecting vortex loops similar to that observed in a chimney flow by Perry & Lim (1978).

To view the lee-side vortices, additional dye was released through the circumferential slit, which uniformly traced the jet boundary layer in the nozzle. Figure 4 shows the result for the $AR = 0.3$ jet at $VR = 3$. Here, it can be seen that the lee-side vortices were formed considerably downstream of the first leading-edge vortex, which further reinforces our vortex loops flow model. Also, instead of one CVP, which is often found in circular jets in cross-flow, low-AR jets possess two CVPs at the sides of the jet column. We refer to the stronger one as the primary CVP, and the weaker one as the secondary CVP. As the jet column became bent in the downstream direction, the primary CVP subsequently entrained the secondary CVP, and became the dominant flow structure in the far field, much like in the circular jet case. This finding suggests that the effects of jet geometry are confined to the near field only, and damped out in the far field, which depends only on the gross jet geometry. Although not shown here, the results for $AR = 0.5$ are similar to those for $AR = 0.3$, except that the interaction of the leading-edge vortices (and hence vortex pairing) is less intense, due probably to the lower curvature of the vortex filament facing the cross-flow, compared to the $AR = 0.3$ jet.

The above observation leads us to propose a vortex skeleton model for the low-AR jets as shown in figure 5. It can be seen that apart from the two CVPs, which are indicated by the double folding of the jet shear layer, the model is similar to that of

https://doi.org/10.1017/S0022112003005925 Published online by Cambridge University Press

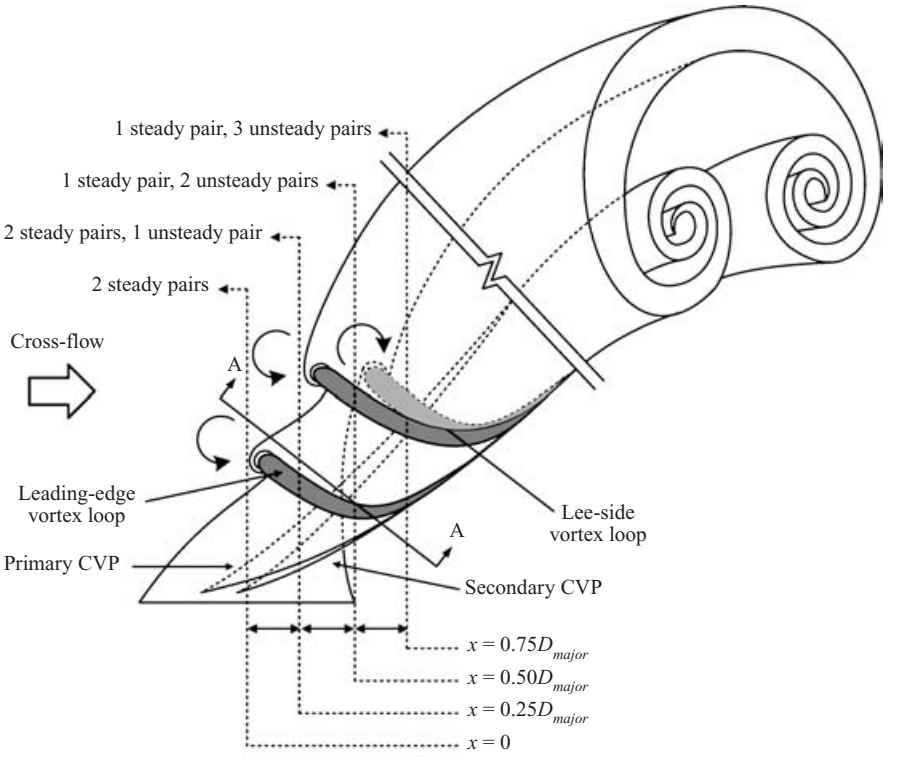


FIGURE 5. Vortex skeleton model of a low-AR jet in cross-flow ($AR = 0.3$ and 0.5). Section A–A indicates a typical location where the flow structures have been sectioned in a plane normal to the jet axis (see figure 6). Vertical broken lines indicate the locations where cross-sections of the structures in a plane normal to the cross flow-direction are taken (see figure 7).

a circular jet in cross-flow proposed by Lim *et al.* (2001). To assess the validity of the model, cross-sectional views of the model in planes normal to the jet trajectory (A–A plane in figure 5) are compared with the corresponding LIF images in figure 6. It can be seen that there is a good agreement between the model and the experiment, except for the presence of an extra CVP near the trailing edge of the jet (see figure 6*b* ii and 6*b* iii). We believe this to be a manifestation of the deformation of the jet column by the cross-flow as the latter closed in at the trailing edge, and did not play a major role in the overall development of the jet structure, as can be seen by its disappearance further downstream. It is perhaps also worth noting that near the jet exit, the secondary CVP was initially slightly better developed than the primary CVP (see figure 6*b* i), but further downstream it is entrained by the stronger primary CVP, as can be see in figure 6(*b* ii). It is not clear why the secondary CVP was initially larger than the primary CVP.

A further validation of the model is displayed in figure 7, where cross-sectional views of the model in planes normal to the cross-flow are compared with the corresponding LIF images. To facilitate the comparison, the expected number of steady and unsteady CVPs is indicated in figure 5, and all the LIF images were captured at the same phase of the leading-edge vortex shedding cycle, which was determined by a time-code card in the video recorder. Generally, there is a good match between the experiment and the model, except for an occasional extra pair of shear layer roll-up vortices, which

https://doi.org/10.1017/S0022112003005925 Published online by Cambridge University Press

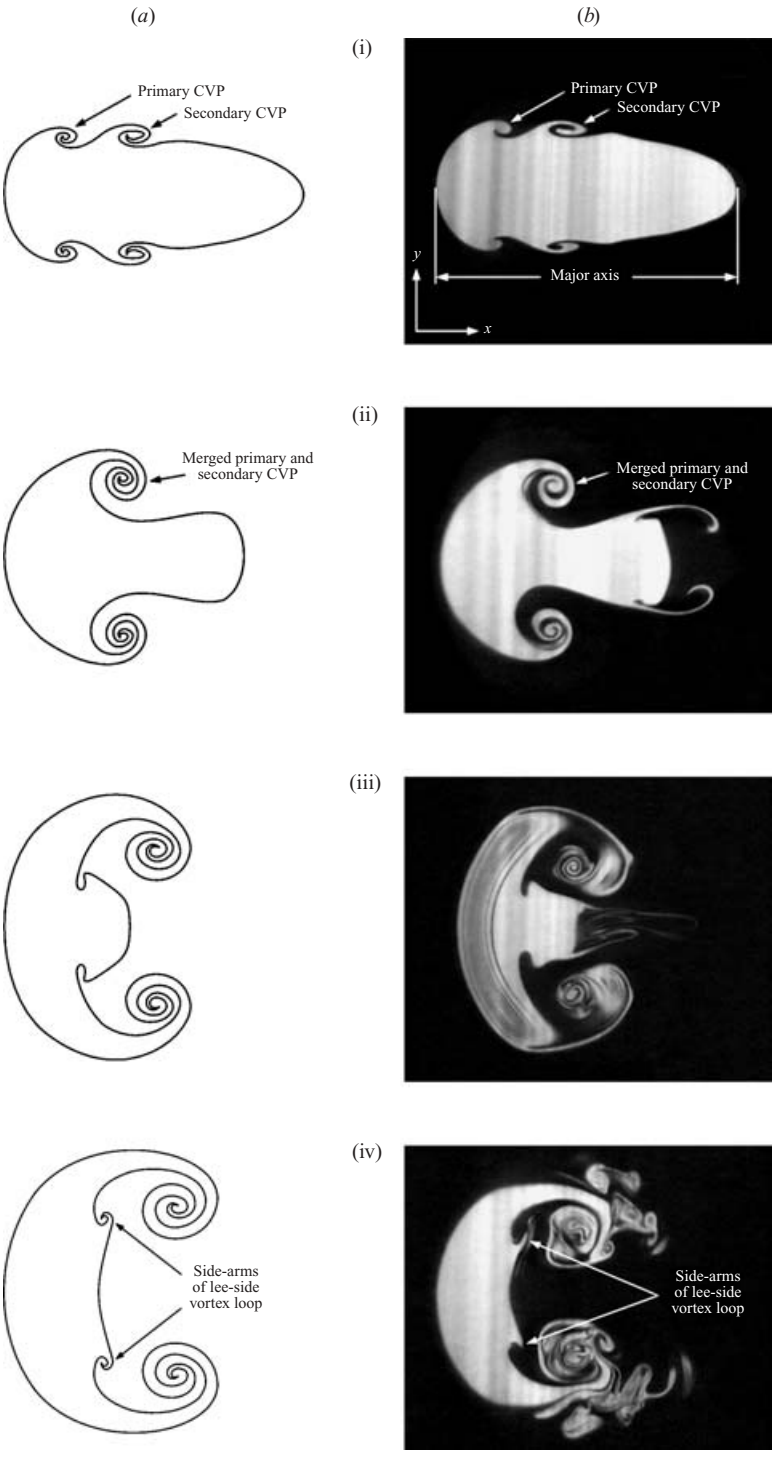


FIGURE 6. Cross-sections of a low-AR jet in planes normal to the mean jet trajectory. (a) Based on the proposed model (section A–A in figure 5). (b) Experimental results ($AR = 0.3$ and $VR = 3$). s is measured along the mean jet trajectory from the jet exit and D_h is the hydraulic diameter of the elliptic jet. (i) $s = 0.5D_h$, (ii) $s = 1.5D_h$, (iii) $s = 2.0D_h$, (iv) $s = 3.0D_h$.

https://doi.org/10.1017/S0022112003005925 Published online by Cambridge University Press

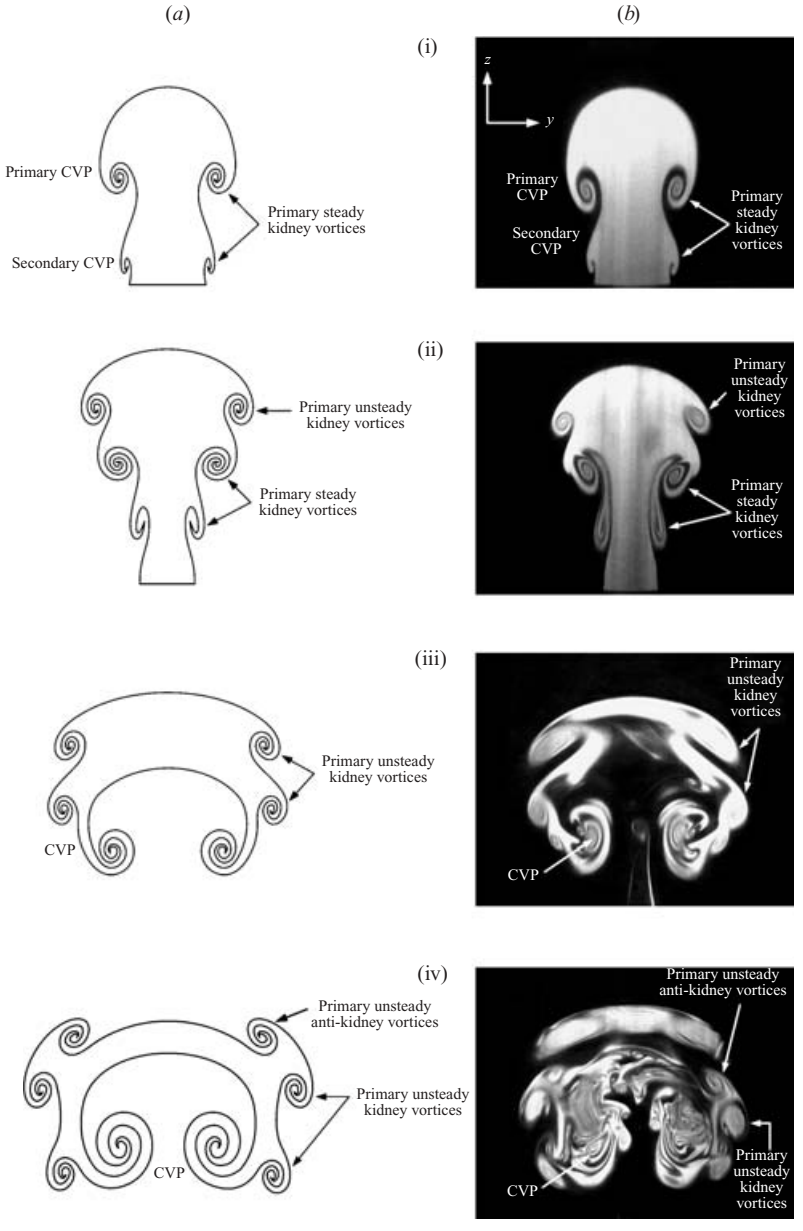


FIGURE 7. Cross-sections of a low-AR jet in a vertical plane normal to the cross-flow at different downstream distances from the jet origin ($x = 0$). (*a*) Based on the proposed model (see broken vertical lines in figure 5). (*b*) Experimental results ($AR = 0.3$ and $VR = 2$). (i) $x = 0$, (ii) $x = 0.25D_{major}$, (iii) $x = 0.50D_{major}$, (iv) $x = 0.75D_{major}$.

appears in the experiment (see figures 7*b* iii and 7*b* iv), but not reflected in the model. We believe the extra roll-up is caused by another leading-edge vortex, which happened to 'stray' into the laser plane.

Figures 7(*b* ii) and 7(*b* iii) clearly show what Haven & Kurosaka (1997) termed 'unsteady upper-deck kidney vortices', or as we prefer to call them, 'primary unsteady kidney vortices'. The decision to use a different nomenclature is based on the necessity

https://doi.org/10.1017/S0022112003005925 Published online by Cambridge University Press

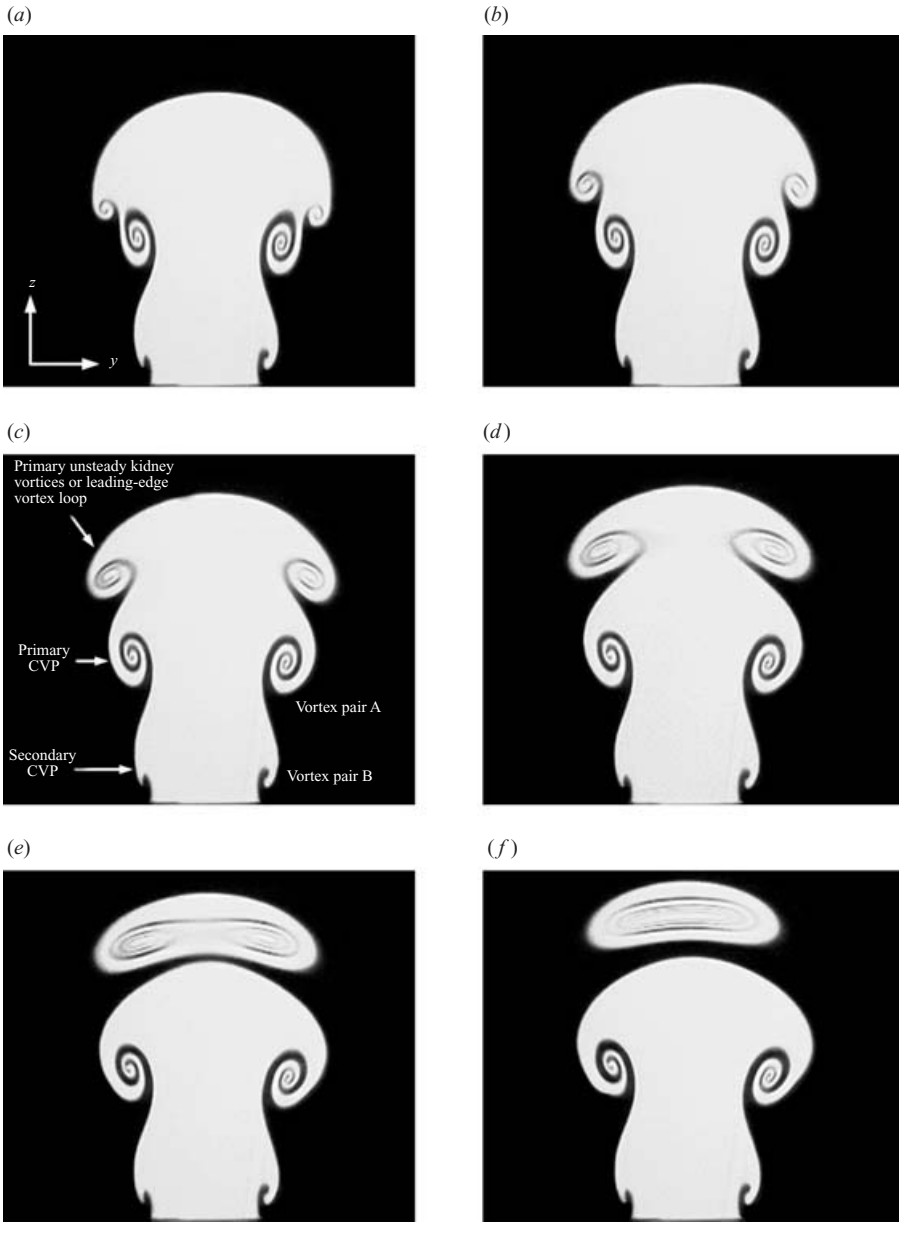


FIGURE 8. LIF images in a vertical plane normal to the cross-flow at $x = 0.25D_{major}$ showing temporal development of a leading-edge vortex (or primary unsteady kidney vortices), primary CVP and secondary CVP (or secondary steady kidney vortices). (*a*) $t = 0$, (*b*) $t = 0.08$ s, (*c*) $t = 0.16$ s, (*d*) $t = 0.24$ s, (*e*) $t = 0.32$ s, (*f*) $t = 0.40$ s.

to differentiate 'primary unsteady kidney vortices' from 'secondary unsteady kidney vortices', which Haven & Kurosaka (1997) did not observe in their experiments. In our interpretation of the flow field, the primary and secondary unsteady vortices emanated from very different flow structures and a distinction is made here to avoid confusion. To have a clearer picture of how the primary unsteady kidney vortices are generated, figure 8 shows the time-sequenced LIF images for the $AR = 0.5$ jet at $VR = 2$, with the

https://doi.org/10.1017/S0022112003005925 Published online by Cambridge University Press

laser sheet located normal to the cross-flow direction at $x = 0.25D_{major}$ downstream of the jet origin. In these pictures, three sets of CVPs arranged in a triple-deck can be clearly seen, with the two pairs closer to the floor exhibiting a steady behaviour. While it is obvious that the larger (vortex pair A) of the two steady vortex pairs is the 'steady lower-deck kidney vortex' referred to by Haven & Kurosaka (1997), it is unclear whether they saw the other pair nearer to the floor (vortex pair B). Viewing a slow-motion replay of the video shows that the two steady vortex pairs are the primary and secondary CVPs depicted in figure 6. While we agree with Haven & Kurosaka (1997) that the uppermost unsteady CVP is the manifestation of the leading-edge vortices passing periodically across the laser sheet, we differ in the interpretation of how these vortices are formed. This issue will be taken up again later.

3.2. *High-aspect-ratio elliptic jets in cross-flow*

3.2.1. *General discussion*

Figure 9 shows the flow structures of a high-AR jet (i.e. $AR = 3$) when dye was released from the upstream injection port. It can be seen that aligning the minor axis of the ellipse with the cross-flow caused a reduction in the regularity of the leading-edge vortices and the intensity of the vortex interaction. Also, the phenomenon of vortex pairing, which is prominent in the low-AR jets, is seldom observed here. This is hardly surprising because the curvature of the leading-edge vortex filaments facing the cross-flow is considerably lower than that in the low-AR jets (see figure 3), which translates into a lower self-induced velocity, and hence less intense vortex interaction.

Although not very obvious in figure 9, detailed observation of the flow structures during the experiment showed that, prior to the formation of the leading-edge vortices, the high-AR jet develops one or more folds on the windward side of the vortex sheet. These folds (the evidence of which will be shown later in LIF images) eventually rolled up into counter-rotating vortex pairs, which we refer to as windward vortex pairs (WVP) in order to differentiate them from the secondary CVP which occur at the side of a low-AR jet column. Although WVPs are smaller and significantly weaker than the primary CVP, their distance from the CVP prevented them from becoming entrained by the primary CVP. This is in contrast to the low-AR jet, where the close proximity of the primary CVP and the secondary CVP resulted in them merging together. Depending on the sense of rotation of the vortex sheet folding, the geometry of the WVP can take any one of the three possible forms, which we label Scenarios 1 to 3 respectively (see figure 10). Which Scenario dominates depends on both AR and VR, and quite often two different Scenarios can exist at the same AR, although not at the same VR, as will be revealed later. As shown in figure 10, both Scenarios 1 and 2 possess one primary CVP, and one WVP with its sense of rotation opposite to that of the primary CVP in Scenario 1, and the same as the primary CVP in Scenario 2. Because there was no noticeable interaction between the WVP and the primary CVP in the high-AR jet, and when the shear layer eventually rolled up to form leading-edge vortices, the WVP was also rolled up by the shear layer. Scenario 3 is a variation of Scenario 2 with two additional WVPs alongside the central WVP (see figure 10c). The existence of Scenario 3 raises the question of whether there are corresponding multiple WVPs in Scenario 1. Such a Scenario is depicted in figure 10(d) as Scenario 4, where three WVPs of opposite rotational sense to Scenario 3 exist along the windward side of the jet shear layer. Although topologically feasible, we did not see this Scenario in any of our experiments. The reason for its absence is not entirely clear to us.

https://doi.org/10.1017/S0022112003005925 Published online by Cambridge University Press

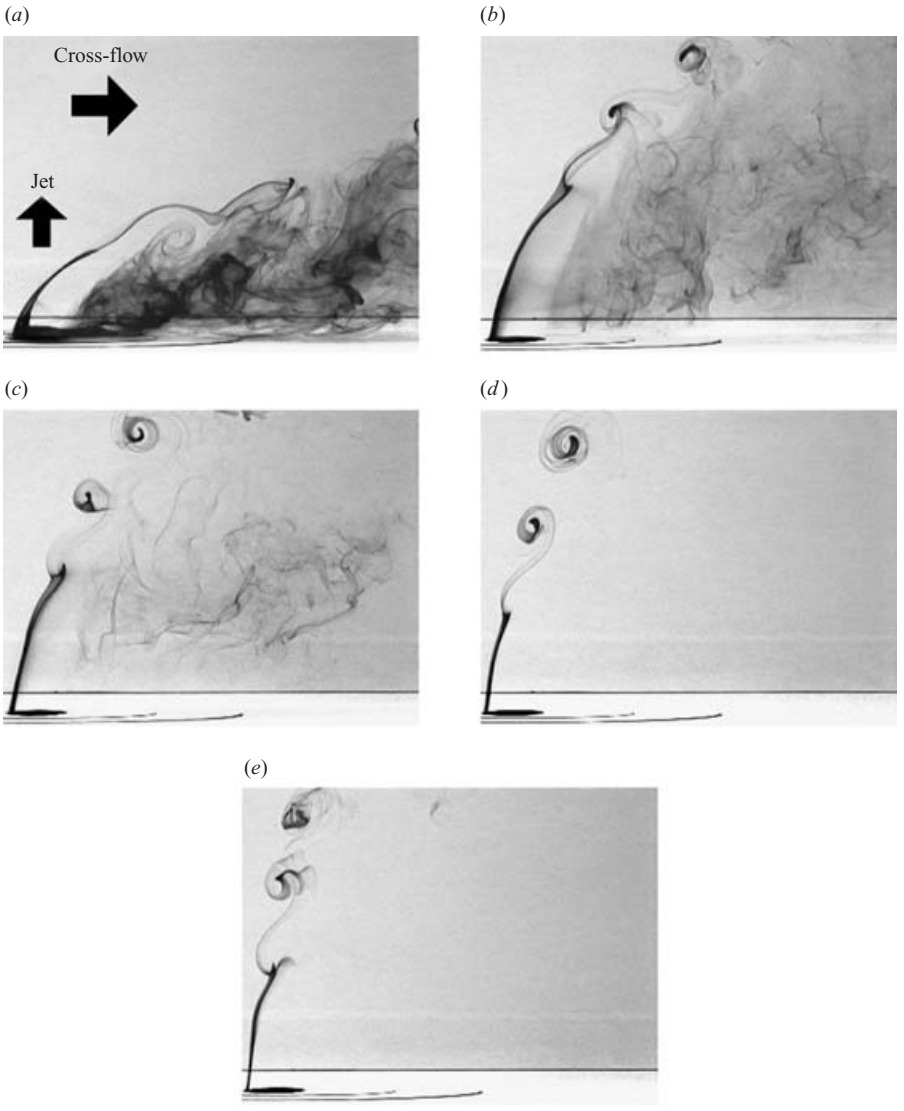


FIGURE 9. Dye pattern of an $AR = 3$ jet for different velocity ratios. The dye was released through a dye port located upstream of the jet exit. (*a*) $VR = 1$, (*b*) $VR = 2$, (*c*) $VR = 3$, (*d*) $VR = 4$, (*e*) $VR = 5$.

We believe that the existence of the WVPs could be due to the 'convex' and 'concave' warping of the leading-edge vorticity similar to that suggested by Haven & Kurosaka (1997). Their transient model of the interaction between the jet and the cross-flow along the windward jet/cross-flow interface could account for the present observations in Scenarios 1 and 2. Scenario 3 (and Scenario 4, for that matter) is merely an extension of Scenarios 1 and 2 as a result of further shear layer instability similar to the one observed by Liepmann & Gharib (1992) for a free circular jet. We agree with Haven & Kurosaka (1997) that the convex and concave warping or folding of the vortex sheet is instrumental in the formation of unsteady kidney and unsteady anti-kidney vortices. However, the similarity ends there because we believe

https://doi.org/10.1017/S0022112003005925 Published online by Cambridge University Press

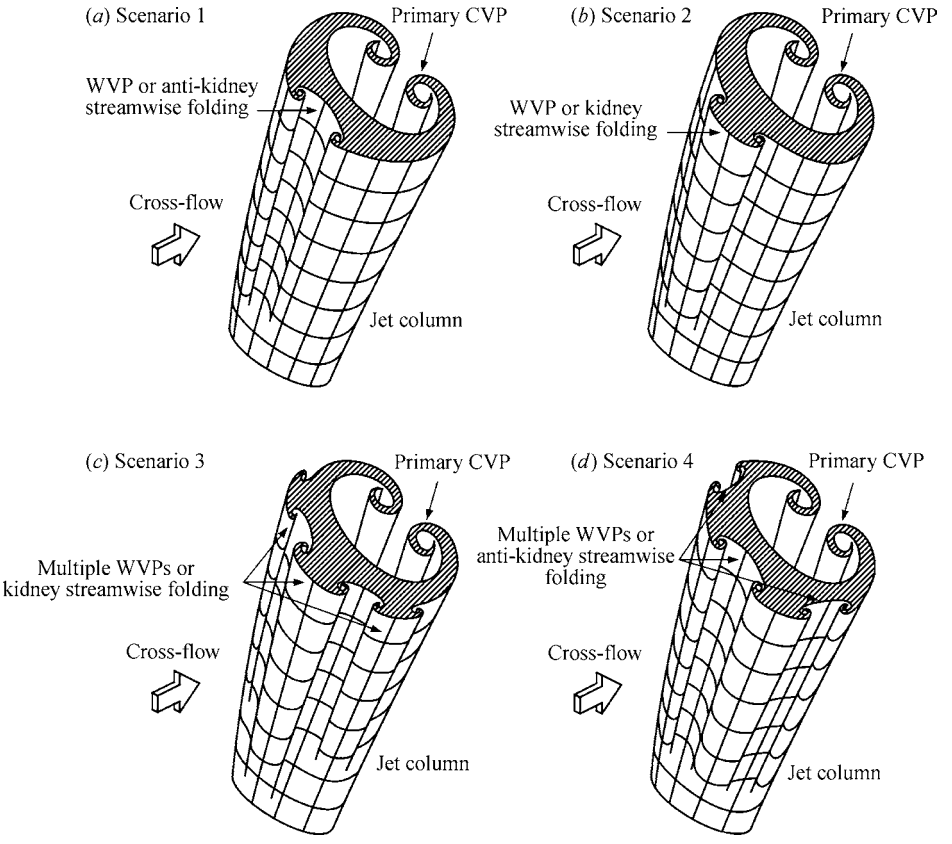


FIGURE 10. Authors' interpretation of the three possible Scenarios for a high-AR jet, depending on the sense of rotation of the WVP. Scenario 1 is responsible for what Haven & Kurosaka (1997) refer to as unsteady anti-kidney vortices, and Scenario 2 is responsible for unsteady kidney vortices. Scenario 3 is a variation of Scenario 2. While not observed in the present study, the hypothetical Scenario 4 (a variation of Scenario 1) is also shown here.

that the subsequent process leading to the formation of these vortices is significantly different from their interpretation. We will discuss this further below.

Before embarking on a detailed discussion of the results, it is important that we clarify some of the terms used in the present paper to avoid confusion with those used by Haven & Kurosaka (1997). They are summarised in table 2. Here, we have sub-divided what Haven & Kurosaka (1997) referred to as 'unsteady kidney vortices' into 'primary unsteady kidney vortices' and 'secondary unsteady kidney vortices' to better reflect the additional flow features that we have observed that were not reported by Haven & Kurosaka (1997). Similarly, the term 'steady kidney vortices' has also been subdivided into 'primary steady kidney vortices' and 'secondary steady kidney vortices'.

Despite the added complexity due to the presence of the WVPs, the process leading to the formation of leading-edge vortices and lee-side vortices for the three Scenarios is found to be similar to that in the low-AR jets, and figure 11 shows the authors' interpretation. The break in the figure is to separate the near-field structures from the far-field structures, which are dominated by the CVP. The expected cross-sections based on the flow models after the WVPs have been formed are shown in sections

https://doi.org/10.1017/S0022112003005925 Published online by Cambridge University Press

Type	Nomenclature used by the present authors	Actual flow structures	Nomenclature used by Haven & Kurosaka (1997)
1	Primary steady kidney vortices	The primary CVP crossing the laser plane. Observed for both low- and high-AR elliptic jets.	Steady kidney vortices
2	Secondary steady kidney vortices	The secondary CVP crossing the laser plane. Here observed for low-AR elliptic jets only.	Not reported
3	Primary unsteady kidney vortices	The leading-edge vortices crossing the laser plane. These vortices will always be observed irrespective of the AR of the elliptic jets, as well as the type of secondary unsteady vortices observed.	Unsteady kidney vortices
4	Secondary unsteady kidney vortices	The WVP(s) 'riding' on top of the jet shear layer or leading-edge vortices as they cross the laser plane. Which type of secondary unsteady vortices prevails depends on the rotational sense of the WVP(s). Here observed for $AR = 3$ elliptic jet only.	
5	Secondary unsteady anti-kidney vortices		Unsteady anti-kidney vortices

TABLE 2. A comparison between the nomenclature used by Haven & Kurosaka (1997) and those used in the present study.

B–B and C–C. For clarity, enlarged views of the WVPs after they have been rolled up by a leading-edge vortex are shown in figure 12(a–c), with the viewing direction aligned with the cross-flow. As will be shown later, the appearance of secondary unsteady kidney and anti-kidney vortices is actually the manifestation of the WVPs travelling across the laser plane.

With the three vortex skeleton models in place, we can now compare them with the experiments.

3.2.2. *Elliptic jet in cross-flow with* $AR = 3$

For the $AR = 3$ jet, the near-field jet structures take on the appearance of either Scenario 1 or Scenario 2, depending on VR. In particular, only Scenario 2 is found when $VR \leqslant 2$, and either Scenario 1 or Scenario 2 is possible when $VR > 2$. This suggests that the jet structures can switch from one Scenario to another, and also means that while Scenario 1 is topologically possible when VR is less than 2, no convincing evidence was observed in the present study.

To check the accuracy of the proposed models, a pseudo-time-sequence of the cross-sectional views of the model for Scenario 1 (viewed in the upstream direction) is compared with the corresponding LIF pictures for a typical $AR = 3$ jet at $x = 0.25D_{minor}$ (see figure 13). For brevity, proposed and experimental cross-sections

https://doi.org/10.1017/S0022112003005925 Published online by Cambridge University Press

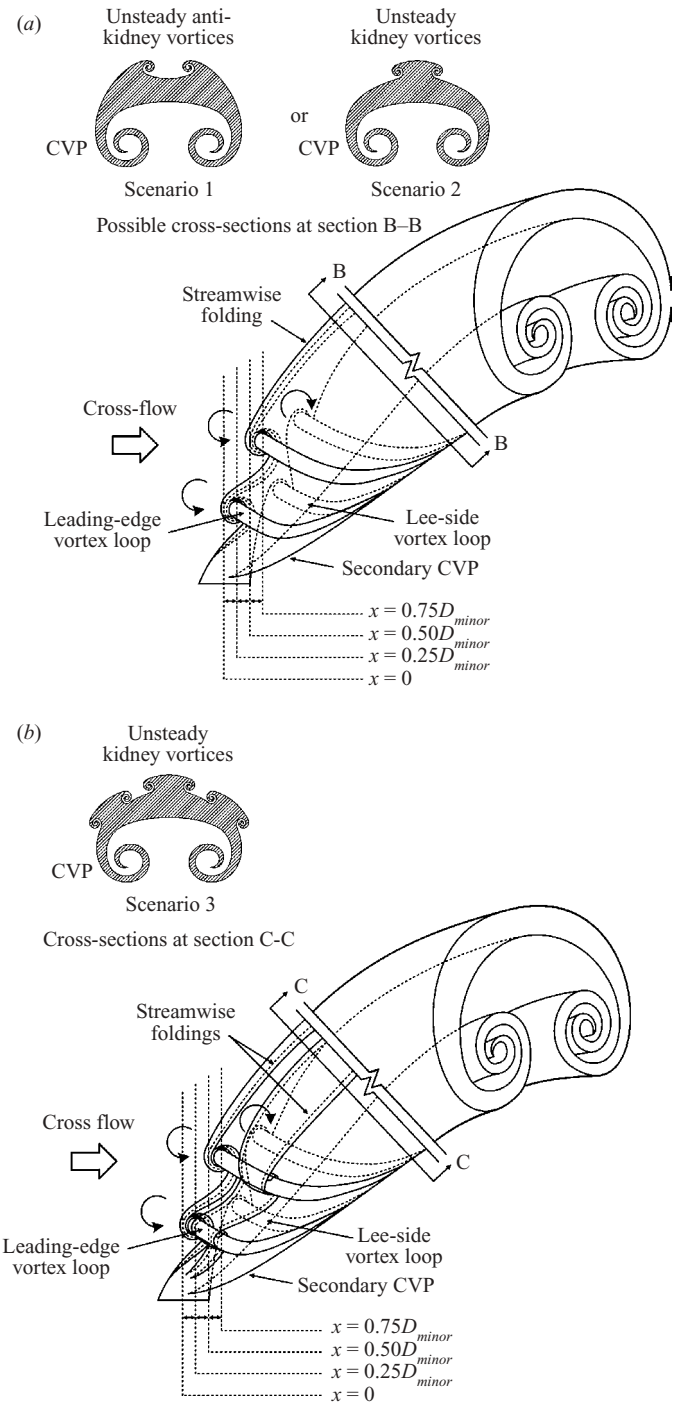


FIGURE 11. Authors' interpretation of a fully developed high-*AR* jet after the shear layer has rolled up into leading-edge vortices. (*a*) Scenario 1 or Scenario 2, (*b*) Scenario 3. The break in each figure is to differentiate the near-field structures from the far-field structures.

https://doi.org/10.1017/S0022112003005925 Published online by Cambridge University Press

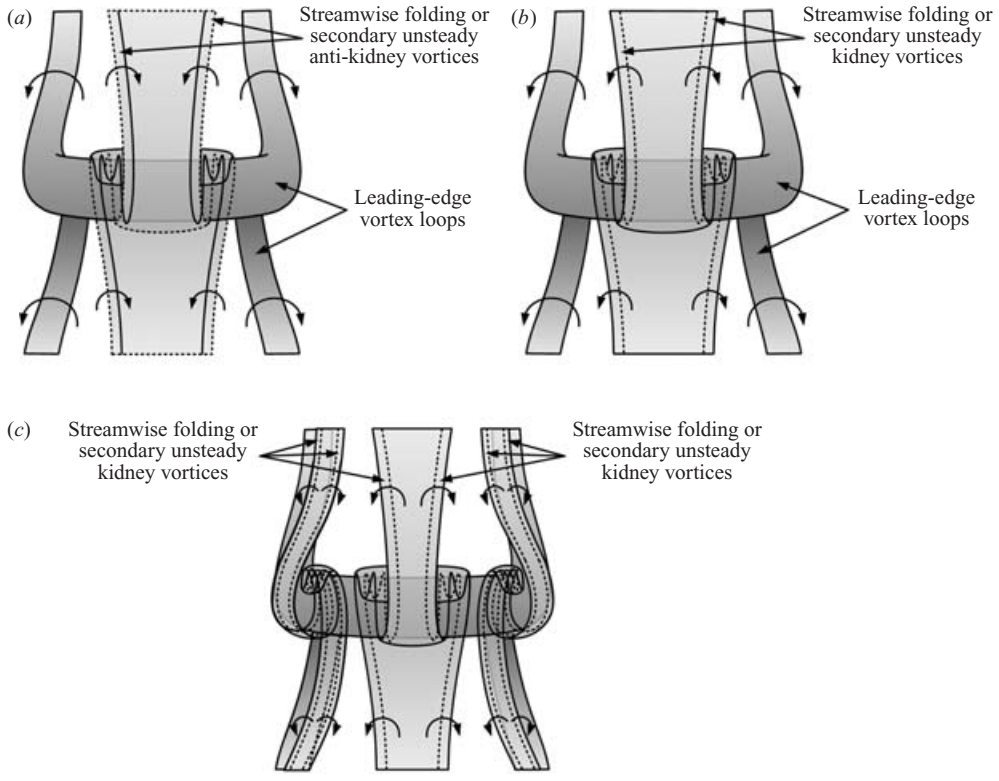


FIGURE 12. Sketches showing how Scenario 1, Scenario 2 and Scenario 3 are rolled up by the leading-edge vortices. Note the opposite sense of rotation of the streamwise folds or WVP in Scenario 1 and Scenario 2.

normal to the mean jet trajectory will not be shown here for the high-AR jets, since the same flow features are also displayed in the cross-sectional views normal to the free stream, although they appear slightly distorted. In obtaining the time-sequence for the model, it is assumed that distance is time-like, meaning that the temporal variation at one location is taken to be the same as the spatial variation at a given instant in time. As can be seen from the figure, the model gives a good representation of the experiment, apart from a minor flow asymmetry, which could be due to flow unsteadiness. Also, because of the manner in which fluorescent dye is introduced into the jet, some of the detailed flow structures have been obscured by the dye and appear as 'blobs' in figures 13(*b* i) and 13(*b* ii). Here, it can be seen that the secondary unsteady anti-kidney vortices are riding on top of the leading-edge vortex, and as they travel across the visualization plane, the secondary unsteady anti-kidney vortices appear to be lifted from the main jet body, revealing their underside (see figure 13*b* iii). Moments later, the side-arms of the leading-edge vortices disappear from the laser plane (see figure 13*b* iv), soon followed by the disappearance of the secondary unsteady anti-kidney vortices, before the cycle is repeated.

The sequence of events for Scenario 2, is similar to that for Scenario 1, except that the secondary unsteady kidney vortices are formed instead (see figure 14). Note how the underside of the secondary unsteady kidney vortices in figure 14(*b* iii) differs in appearance from that of the secondary unsteady anti-kidney vortices in figure 13(*b* iii).

https://doi.org/10.1017/S0022112003005925 Published online by Cambridge University Press

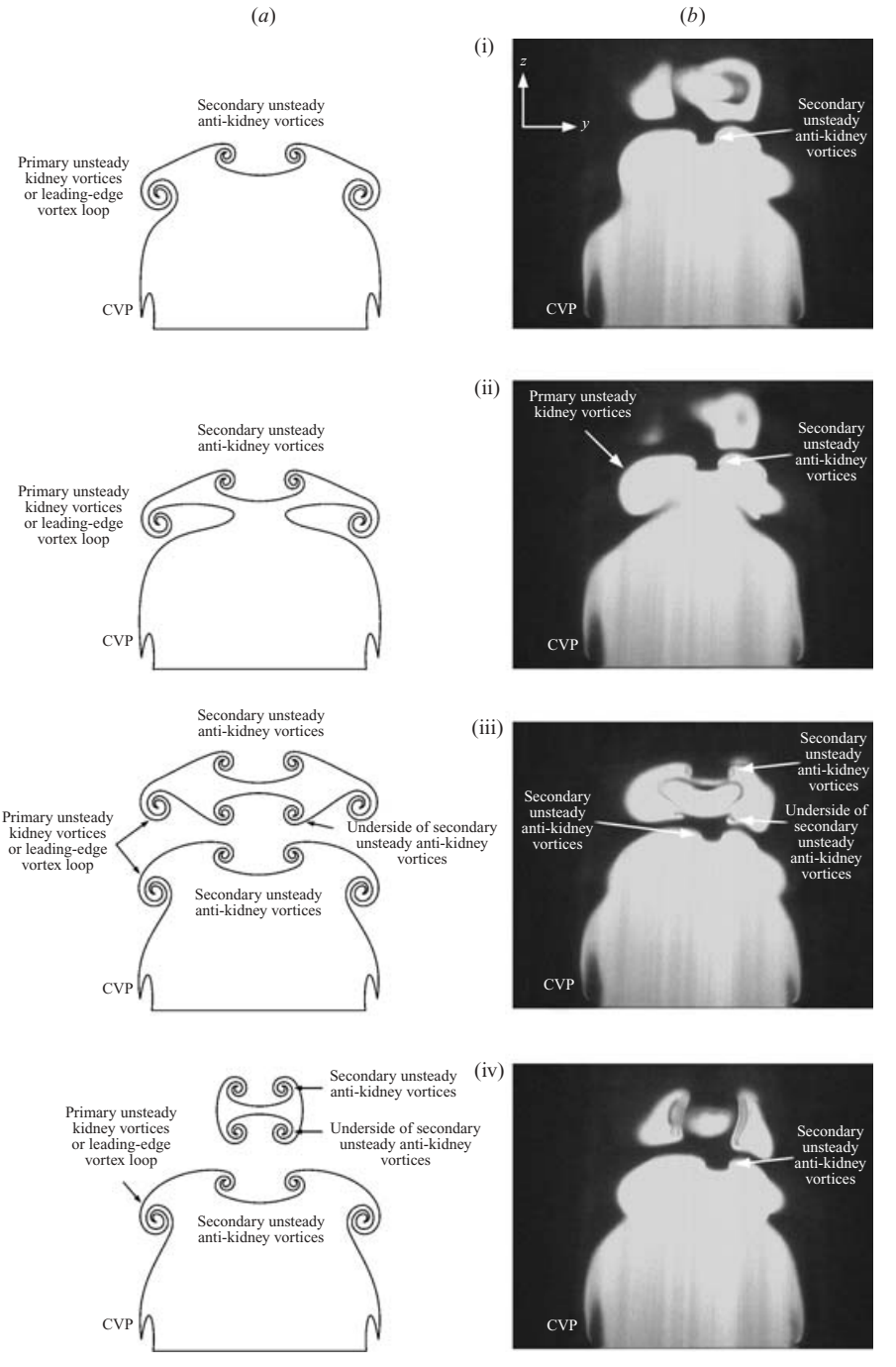


FIGURE 13. Time-sequence cross-sections of a jet with Scenario 1 in a plane normal to the cross-flow at $x = 0.25D_{minor}$. (*a*) Based on the model, (*b*) experiment ($AR = 3$, $VR = 4$). Note how the anti-kidney vortices riding on the top of the leading-edge vortex loop in (i) are subsequently lifted by the vortex loop at a later time in (iii) and (iv). This finding is consistent with the observation of Haven & Kurosaka (1997). (i) $t = 0$, (ii) $t = 0.04$ s, (iii) $t = 0.12$ s, (iv) $t = 0.16$ s.

https://doi.org/10.1017/S0022112003005925 Published online by Cambridge University Press

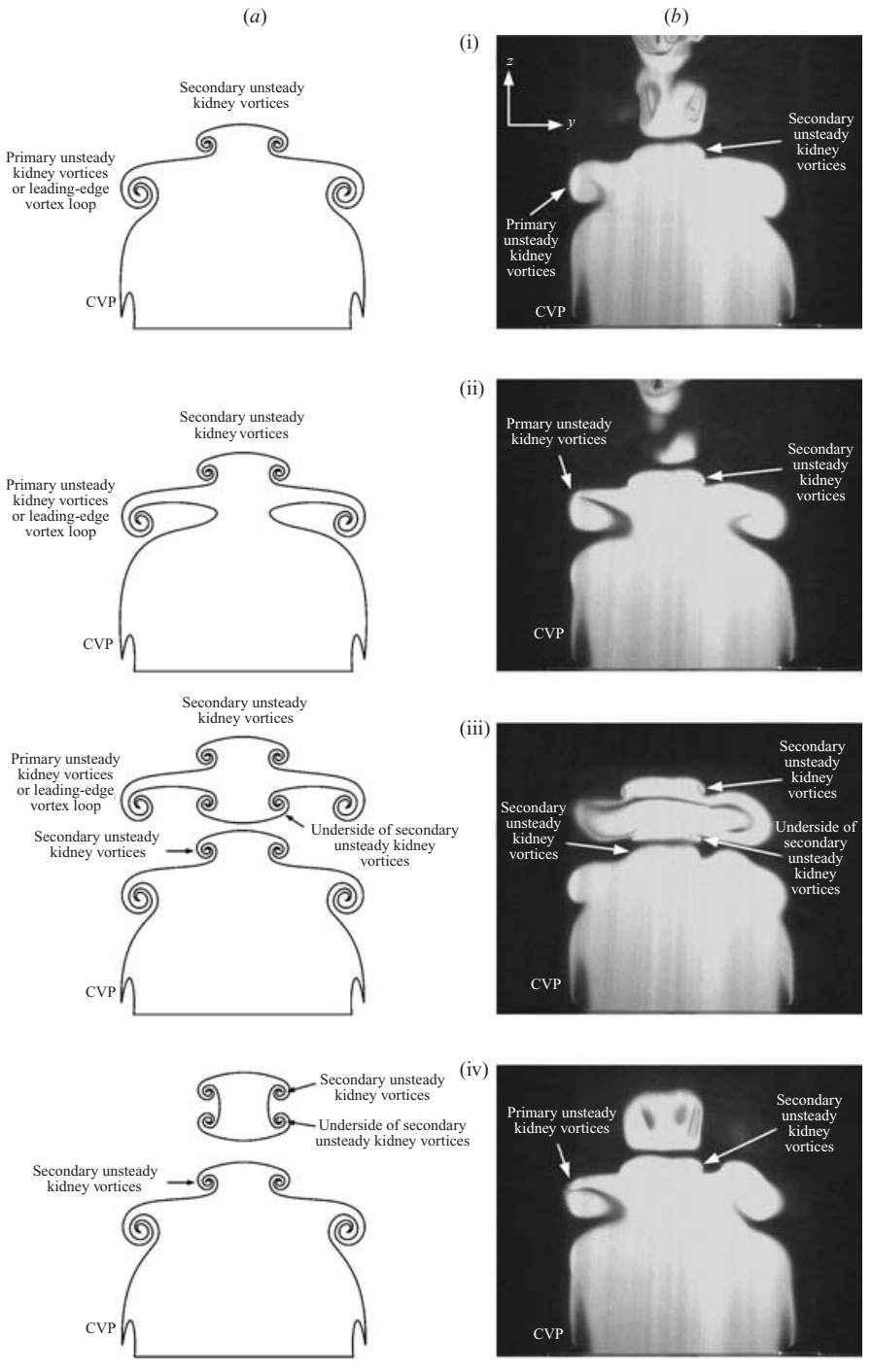


FIGURE 14. Time-sequence cross-sections of a jet with Scenario 2 in a plane normal to the cross-flow at $x = 0.25D_{minor}$. (*a*) Based on the model, (*b*) experiment ($AR = 3$, $VR = 4$). (i) $t = 0$, (ii) $t = 0.08$ s, (iii) $t = 0.12$ s, (iv) $t = 0.2$ s.

https://doi.org/10.1017/S0022112003005925 Published online by Cambridge University Press

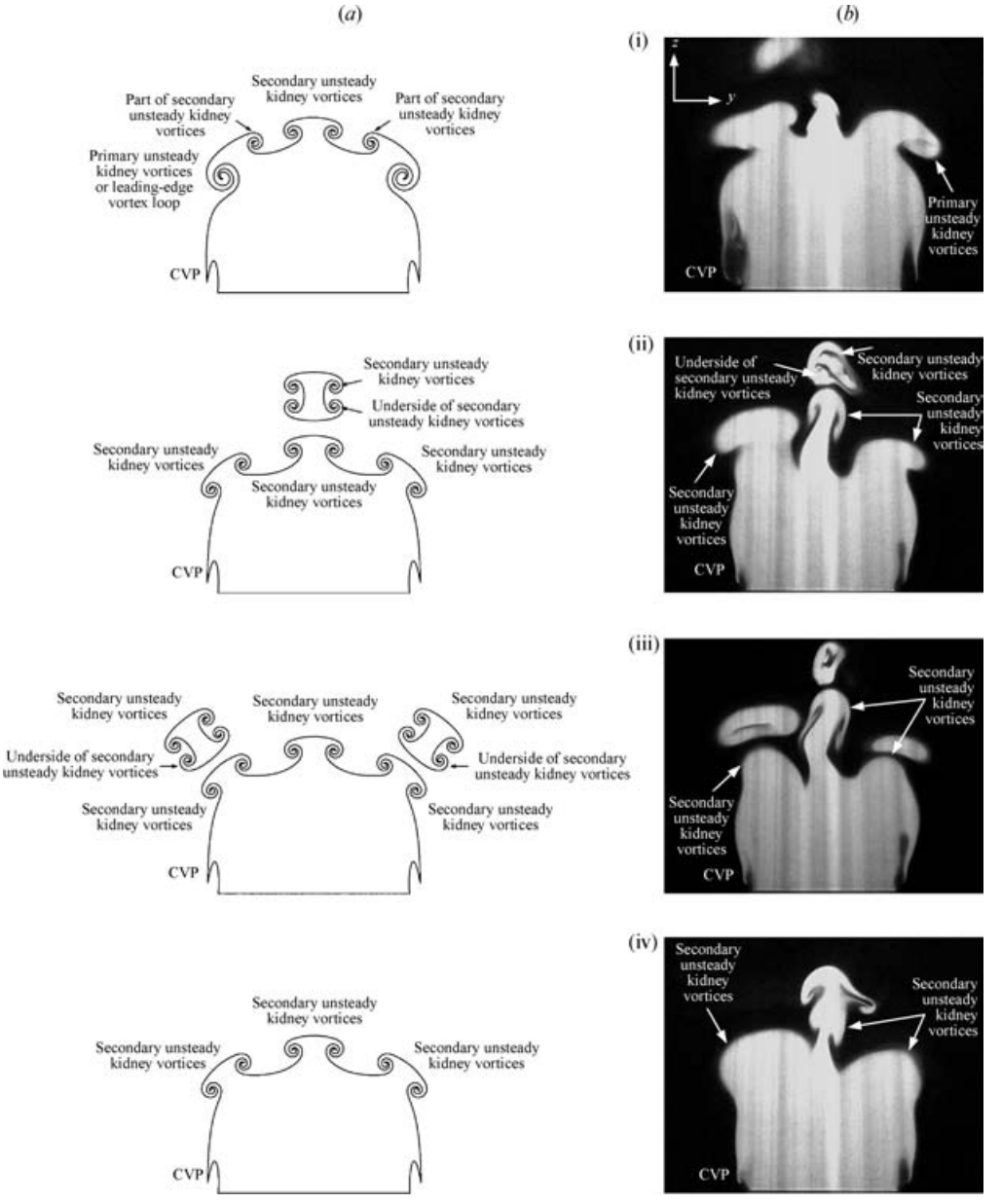


FIGURE 15. Time-sequence cross-sections of a jet with Scenario 3 in a plane normal to the cross-flow at $x = 0.25D_{minor}$. (*a*) Based on the model, (*b*) experiment ($AR = 2$, $VR = 3$). (i) $t = 0$, (ii) $t = 0.08$ s, (iii) $t = 0.12$ s, (iv) $t = 0.2$ s.

As noted earlier, while we agree with Haven & Kurosaka (1997) that the convex and concave warping or folding of the vortex sheet is instrumental in the formation of unsteady kidney and unsteady anti-kidney vortices, we differ on the mechanism by which these vortices are formed. They considered the appearance of unsteady kidney vortices to be a cross-plane manifestation of leading-edge vortices caused by convex warping of the windward-side vortex sheet, meaning that the frontal vortex

https://doi.org/10.1017/S0022112003005925 Published online by Cambridge University Press

<table>
<tr><td rowspan="2">AR</td><td colspan="5">VR</td></tr>
<tr><td>1</td><td>2</td><td>3</td><td>4</td><td>5</td></tr>
<tr><td>0.3</td><td colspan="5" rowspan="2">Topologically similar to a circular jet in cross flow, except for the presence of a secondary CVP near the jet exit.</td></tr>
<tr><td>0.5</td></tr>
<tr><td>1.0</td><td>Wake-like structures</td><td colspan="4">Circular jet in a cross-flow (see model in Lim et al. 2001)</td></tr>
<tr><td>2.0</td><td colspan="2">Scenario 2</td><td colspan="3">Scenario 2 and 3</td></tr>
<tr><td>3.0</td><td colspan="2">Scenario 2</td><td colspan="3">Scenario 1 and 2</td></tr>
</table>

TABLE 3. A summary of the possible jet structures existing for low- and high-AR elliptic jets in cross-flow for various velocity ratios. Note that for high-AR, apart from the presence of WVP, the flow structure is also topologically similar to that of a circular jet in cross-flow.

sheet first undergoes convex warping, and then the formation of the leading-edge vortices follows the contour of the warping (see figure 18 in Haven & Kurosaka 1997). Likewise, they attributed the formation of unsteady anti-kidney vortices to the concave warping of the vortex sheet before the sheet rolls up to form leading-edge vortices. Although Haven & Kurosaka's (1997) interpretation of the formation of these vortices is topological feasible, we did not see it in any of our experiments.

In contrast, we believe that the convex or concave warping of the vortex sheet is responsible for the formation of WVP only, and that the leading-edge vortex filaments do not follow the contour of the vortex sheet as suggested by Haven & Kurosaka (1997). If one examines the results of Haven & Kurosaka (1997) closely, it can be seen that their unsteady kidney and unsteady anti-kidney vortices formed very differently from each other and could not have all originated from the same leading-edge vortices. Their side-view photographs for low- and high-AR elliptic jets in cross-flow all showed shedding of the leading-edge vortices; therefore cross-plane LIF visualizations of these leading-edge vortices should always yield at least one pair of unsteady kidney vortices. This implies that the source of their unsteady anti-kidney and the second pair of unsteady kidney vortices has to be elsewhere, which in our experiment is the WVP discussed earlier. Whether the difference in the observation is due to the low VR used in their experiment ($VR = 0.4$ to 2) remains unclear. In our case, we believe that the WVP are much weaker than the leading-edge vortices, as can be inferred from the manner in which they are rolled up by the leading-edge vortices (see figures 13*b* iii and 14*b* iii). Unfortunately, we were unable to obtain the relative strength of the WVP and the leading-edge vortices because the presence of a large cross-plane velocity component makes PIV measurements difficult. Nevertheless, the results of Haven & Kurosaka (1997), which were obtained at a lower VR indicate that the circulation of the secondary unsteady anti-kidney vortices (i.e. WVP in the present study) is significantly lower than that of the primary unsteady kidney vortices (i.e. leading-edge vortices in the present study) with the maximum value of the former approximately 40% lower than that of the latter. This finding supports our observation.

https://doi.org/10.1017/S0022112003005925 Published online by Cambridge University Press

3.2.3. *Elliptic jet in cross-flow with* $AR = 2$

When AR is reduced to 2, Scenario 2 is still dominant at low VR. But at $VR \geqslant 3$, both Scenarios 2 and 3 are possible. This is in contrast to the results of Haven & Kurosaka (1997) for the same AR, where they reported the presence of Scenario 1 only. As mentioned earlier, Scenario 3 is only an extension of Scenario 2, with two additional WVPs (see figure 10*c*). LIF images depicting the existence of Scenario 3 are shown in figure 15, which compare well with the sectional view of our vortex skeleton model. Minor variations between the experiments and the model are caused by general flow unsteadiness.

Table 3 shows a summary of the possible jet structures that exist for the low- and high-AR elliptic jet in cross-flow for VR from 1 to 5 considered in the present study.

4. Conclusions

Experiments have been conducted to study the flow structures of an elliptic jet in cross-flow for a range of jet aspect ratio and velocity ratio, and the results show that the effects of aspect ratio are significant only in the near field, and eventually damped out in the far field which depends only on gross jet geometry. For low-AR elliptic jets, the near field is dominated initially by two CVPs, which subsequently merged into one further downstream. For high-AR elliptic jets, only one CVP is found throughout the jet column, but the shear layer at the jet/cross-flow interface in the near field develops one or more WVP(s) depending on AR and VR. These WVPs can evolve into what Haven & Kurosaka (1997) referred to as unsteady kidney or unsteady anti-kidney vortices. In particular, the WVP with the same sense of rotation as the primary CVP evolves into unsteady kidney vortices (Scenario 2), and the one with the opposite sense of rotation leads to unsteady anti-kidney vortices (Scenario 1). Under some circumstances, Scenario 2 may undergo further instability and form two additional WVPs with the same sense of rotation as the primary CVP, in which case the end result is a series of interconnecting unsteady kidney vortices (Scenario 3). While Scenario 2 is found for all the high-aspect-ratio jets (i.e. $AR = 2$ and 3), Scenario 1 is found for the $AR = 3$ elliptic jet only, and Scenario 3 for the $AR = 2$ elliptic jet only. It is believed that the WVPs originate from the convex or concave warping of the vortex sheet as suggested by Haven & Kurosaka (1997), although we differ in our interpretation on how unsteady kidney and anti-kidney vortices are formed. Despite the influence of the jet geometry on the near-field structures, the mechanism leading to the formation of the large-scale structures (i.e. leading-edge vortices and lee-side vortices) for all elliptic jets follows a process similar to that in a circular jet in cross-flow (see Lim *et al.* 2001).

This project is financially supported by the National University of Singapore Research Grant (No: RP950638)

REFERENCES

Ajersch, P., Zhou, J. M., Ketler, S., Salcudean, M. & Gartshore, I. S. 1997 Multiple jets in a crossflow: Detailed measurements and numerical simulations. *Trans. ASME: J. Turbomach.* **119**, 330–342.

Coelho, S. L. V. & Hunt, J. C. R. 1989 The dynamics of the near-field of strong jets in crossflows. *J. Fluid Mech.* **200**, 95–120.

Fearn, R. & Weston, R. P. 1974 Vorticity associated with a jet in a cross flow. *AIAA J.* **12**, 1666–1671.

https://doi.org/10.1017/S0022112003005925 Published online by Cambridge University Press

Findlay, M. J., Salcudean, M. & Gartshore, I. 1999 Jets in a crossflow: Effects of geometry and blowing ratio. *Trans. ASME*: *J. Fluids Engng* **121**, 373–378.

Fric, T. F. & Roshko, A. 1994 Vortical structure in the wake of a transverse jet. *J. Fluid Mech.* **279**, 1–47.

Gogineni, S., Goss, L. & Roquemore, M. 1998 Manipulation of a jet in cross flow. *Expl Thermal Fluid Sci.* **16**, 209–219.

Haven, B. A. & Kurosaka, M. 1997 Kidney and anti-kidney vortices in crossflow jets. *J. Fluid Mech.* **352**, 27–64.

Kamotani, Y. & Greber, I. 1972 Experiments on a turbulent jet in a cross flow. *AIAA J.* **10**, 1425–1429.

Kelso, R. M., Lim, T. T. & Perry, A. E. 1996 An experimental study of round jets in cross-flow. *J. Fluid Mech.* **306**, 111–144.

Kelso, R. M. & Smits, A. J. 1995 Horseshoe vortex systems resulting from the interaction between a laminar boundary layer and a transverse jet. *Phys. Fluids* **7**, 153–158.

Liepmann, D. & Gharib, M. 1992 The role of streamwise vorticity in the near-field entrainment of round jets. *J. Fluid Mech.* **245**, 643–668.

Lim, T. T., New, T. H. & Luo, S. C. 2001 On the development of large-scale structures of a jet normal to a cross flow. *Phys. Fluids* **13**, 770–775.

Margason, R. J. 1993 Fifty years of jet in crossflow research. *Computational and Experimental Assessment of Jets in Cross Flow*. *AGARD-CP*-534, Winchester, UK.

Moussa, Z. M., Trischka, J. W. & Eskinazi, S. 1977 The near-field in the mixing of a round jet with a cross stream. *J. Fluid Mech.* **80**, 49–80.

New, T. H., Lim, T. T. & Luo, S. C. 1999 On the effects of velocity profiles on the topological structures of a jet in cross flow. *TSFP-1 Proc.* pp. 647–652.

Perry, A. E. & Lim, T. T. 1978 Coherent structures in coflowing jets and wakes, *J. Fluid Mech.* **88**, 451–463.

Scorer, R. S. 1958 *Natural Aerodynamics*. Pergamon.

Yuan, L. L., Street, R. L. & Ferziger, J. H. 1999 Large eddy simulation of a round jet in a crossflow. *J. Fluid Mech.* **379**, 71–104.

Zaman, K. B. M. Q. & Foss, J. K. 1997 The effect of vortex generators on a jet in a cross-flow. *Phys. Fluids* **9**, 106–114.

https://doi.org/10.1017/S0022112003005925 Published online by Cambridge University Press